Gate-tunable spectrum and charge dispersion mitigation in a graphene superconducting qubit

Nicolas Aparicio,[1] Simon Messelot,[1] Edgar Bonet-Orozco,[1] Eric Eyraud,[1]
Kenji Watanabe,[2] Takashi Taniguchi,[3] Johann Coraux,[1] and Julien Renard[1,*]

[1] *Univ. Grenoble Alpes, CNRS, Grenoble INP, Institut Néel, 38000 Grenoble, France*

[2] *Research Center for Electronic and Optical Materials, National Institute for Materials Science, 1-1 Namiki, Tsukuba 305-0044, Japan*

[3] *Research Center for Materials Nanoarchitectonics, National Institute for Materials Science, 1-1 Namiki, Tsukuba 305-0044, Japan*

Abstract

Controlling the energy spectrum of quantum-coherent superconducting circuits, i.e. the energies of excited states, the circuit anharmonicity and the states' charge dispersion, is essential for designing performant qubits. This control is usually achieved by adjusting the circuit's geometry. In-situ control is traditionally obtained via an external magnetic field, in the case of tunnel Josephson junctions. More recently, semiconductor-weak-links-based Josephson junctions have emerged as an alternative building block with the advantage of tunability via the electric-field effect. Gate-tunable Josephson junctions have been succesfully integrated in superconducting circuits using for instance semiconducting nanowires or two-dimensional electron gases. In this work we demonstrate, in a graphene superconducting circuit, a large gate-tunability of qubit properties: frequency, anharmonicity and charge dispersion. We rationalize these features using a model considering the transmission of Cooper pairs through Andreev bound states. Noticeably, we show that the high transmission of Cooper pairs in such weak link strongly suppresses the charge dispersion. Our work illustrates the potential for graphene-based qubits as versatile building-blocks in advanced quantum circuits.

INTRODUCTION

Microwave superconducting quantum circuits rely on the existence of a lossless nonlinear inductive element: the Josephson junction. In the majority of the devices, a tunnel junctions is used [1, 2]. Aternatives, such as disordered superconductors, have been explored for instance to promote wave mixing in a travelling wave parametric amplifier [3], or to build transmon and fluxonium qubits [4, 5]. Another alternative is to revisit the junction itself and replace the tunnel barrier by a conducting material. If its conduction can be tuned by the electric-field effect, this would allow to suppress the need for magnetic field tunability, which is traditionally used when dealing with tunnel Josephson junctions.

Using such so-called hybrid junctions, gate-tunable qubits [6–9] and parametric amplifiers [10–13] have been demonstrated. Semiconducting nanowires were first employed as the weak link. Planar materials are promising alternatives offering a variety of patterning options. Accordingly, two-dimensional (2D) electron gases have been used, including semiconducting

* julien.renard@neel.cnrs.fr

quantum wells [14, 15] or the semi-metal graphene [16, 17]. In all these qubits, it was for instance possible to tune, with the gate voltage, the frequency of the transition to the first excited state by one to few GHz [14, 16, 18].

These hybrid junctions expectedly operate in a regime much different from that typical of Josephson tunnel junctions – Cooper pairs are simply not transported the same way across them. This has strong consequences on the qubit properties. In this work, we present the detailed spectroscopy of a charge qubit based on a gate-tunable graphene Josephson junction. We extract the energy spectrum, its anharmonicity, and the levels' charge dispersion. We analyze these characteristics using the Hamiltonian of a superconducting quantum point contact that takes into account the gate-dependent transmission of different channels as well as Andreev bound states from both branches across the superconducting gap. We accordingly relate the measured quantities to the offset charge as well as the gate-tunable Josephson energy and junction's transmission. We find that the large transmission reduces the charge dispersion, which could allow the design of highly-coherent qubits in the future.

CIRCUIT DESIGN

Measurements were performed in a dilution refrigerator at $\sim$ 25 mK on two different charge qubit-like devices (Q_1 and Q_2, refer to Appendix A for details on their fabrication), each consisting of [see Fig. 1(a)] a graphene-based Josephson junction shunted to ground by a large capacitance (C_{S}). Both circuits are coupled to a coplanar $\lambda/2$ waveguide (CPW) readout resonator via a C_{qr} capacitance (itself coupled to a transmission line thanks to a C_{c} capacitance), and to a drive line (via a C_{d} capacitance) fed with both an AC and DC bias V_{j} provided by a cryogenic bias-tee. The peculiarity here is the gate control (V_{g}) of the Josephson junctions, ensured by a C_{g} capacitance; no magnetic field is used to control the critical current. The primary effect of V_{g} will be to control the Josephson energy (E_{J}) by tuning the critical current of the graphene-based junction [16, 19, 20]. The two devices differ by the shape of their top-gates [see Fig. 1(c,d)] and the values of the capacitances, such that the quality factor (Q_{c}) and charging energy (E_{C}) are respectively larger (1.30×10^4 vs 4.09×10^3) and smaller (343 MHz vs 516 MHz) for Q_1 than for Q_2 (see Table I in Appendix A). Note that the charge dispersion, which we will discuss in details, is highly dependent on the charging energy. The resonant frequency f_{r} of the readout resonator is similar for the two devices, 6.95 GHz (Q_1) and 6.79 GHz (Q_2).

The yield for device fabrication is high, and we reproducibly obtain graphene Josephson junctions with critical currents of a few tens of nA, which is the targeted range for qubits. Precise control of the qubits' Josephson energy by circuit design is nevertheless practically more delicate than with conventionnal tunnel junctions. This is however mitigated by the gate tunability, which authorizes fine adjustments.

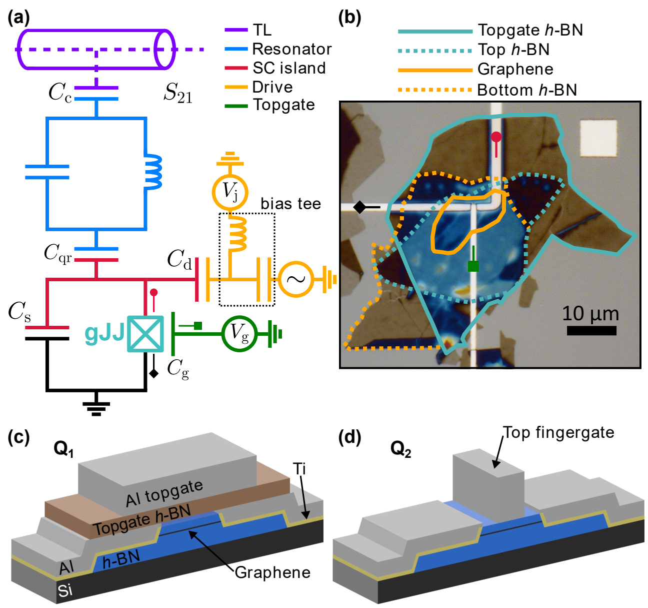

FIG. 1. Devices description. (a) Electrical circuit diagram of a charge qubit made of a graphene Josephson junction (gJJ) shunted to ground by a C_S capacitance, and coupled to a readout resonator by a C_{qr} capacitance, a drive line by a C_d capacitance, and a gate line by a C_g capacitance to control conduction through graphene. The qubit superconducting island is defined by the superconducting leads (red) between the junction and the C_S capacitance. The qubit is read out by probing the transmission scattering parameter, S_{21}, of a transmission line (TL) coupled to a microwave resonator by a C_c capacitance. (b) Optical micrograph of the h-BN/graphene/h-BN heterostructure of device Q_1. (c,d) Schematics of the top-gated gJJs side-contacted to the Ti/Al superconducting electrodes.

CIRCUIT MODEL HAMILTONIAN

Figure 2(a) shows the energy levels within the parabolic potential of the quantum harmonic oscillator (black), and those within the potential of the so-called transmon qubit (red), in which the linear inductor is replaced by a nonlinear one, a Josephson junction. In tunnel Josephson junctions, the coherent tunneling of Cooper pairs is well described by the traditional Josephson Hamiltonian $\hat{H}_{\mathrm{TJ}} = -E_{\mathrm{J}} \cos\left(\hat{\varphi}\right)$, where E_{J} is the junction's Josephson energy and $\hat{\varphi}$ the phase operator. When the weak link is not a tunnel barrier, for example a semiconductor, a metal or a semi-metal (graphene), transmission of Cooper pairs from one electrode to the other is instead described using the concept of Andreev bound states (ABSs), involving electron-hole states within the weak link [21–27] (see Appendix B for details).

To describe our graphene-based junctions (see Supplemental Material [28]), we use a Hamiltonian adapted from a superconducting quantum point contact (QPC) model [29]:

$$\hat{H} = 4E_{\mathrm{C}}\left(\hat{n} - n_{\mathrm{g}}\right)^2 + \Delta \begin{pmatrix} \cos\left(\frac{\hat{\varphi}}{2}\right) & \sqrt{r}\sin\left(\frac{\hat{\varphi}}{2}\right) \\ \sqrt{r}\sin\left(\frac{\hat{\varphi}}{2}\right) & -\cos\left(\frac{\hat{\varphi}}{2}\right) \end{pmatrix}. \tag{1}$$

Here, $\hat{n}$ and $\hat{\varphi}$ are the (conjugated) operators representing the number of Cooper pairs within the superconducting island [red portion of the circuit in Fig. 1(a)] and the phase across the junction; n_{g} is the island's charge offset. Crucially here, the 2×2 matrix encodes the contribution of both the ground and excited ABSs, which are coupled by backscattering, with $r = 1 - \tau$ and τ the channel transmission. In a 2D graphene weak link, however, there is a priori a certain number of conduction channels, N_{C} (that depends on V_{g}, see Supplemental Material [28]), each having a given transmission (V_{g}-dependent too). This seems at odds with the QPC picture, yet the few highest-transmission conduction channels are expected to dominate the Josephson energy E_{J} of the graphene-based junction. To limit the number of unknown parameters, we assume $N_{\mathrm{C}}\left(V_{\mathrm{g}}\right)$ independent ABSs of transmission τ (that depends on V_{g}), which is equivalent to $N_{\mathrm{C}}\left(V_{\mathrm{g}}\right)$ independent QPCs in parallel. This should be seen as an effective model not meant to describe the details of the junction, in particular its precise geometry. We can expect this model to hold at large doping and we will discuss later its limitation near the charge neutrality point. In this picture, the junction has consequently a gate-dependent Josephson energy $E_{\mathrm{J}}\left(V_{\mathrm{g}}\right) = \frac{\Delta N_{\mathrm{C}}(V_{\mathrm{g}})\tau(V_{\mathrm{g}})}{4}$. With these in mind, we numerically solve Hamiltonian 1 in the charge basis (rather than the phase basis, as it is usually done [30]), as detailed in Supplemental Material [28], to compute the energy spectrum and extract relevant experimental parameters such as charge dispersion and anharmonicity. The method for extracting the model parameters (E_J, τ) from the measured data is presented in Supplemental Material [28].

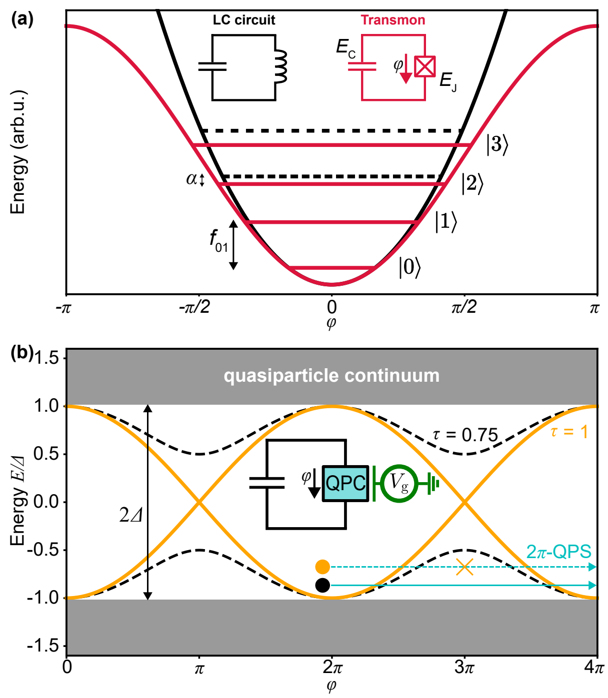

FIG. 2. Superconducting quantum point contact (QPC) model for a qubit based on a gate-tunable weak link between two superconducting electrodes. (a) Energy potential of the quantum harmonic oscillator (black) and the transmon qubit (red). (b) Josephson potential of a QPC. When the transmission τ is below unity (black dotted line), 2π-quantum phase slips (2π-QPSs) can occur, which is directly responsible for charge dispersion. For $\tau = 1$ (solid orange line), the two ABS branches cross and 2π-QPS is forbidden, leading to a vanishing charge dispersion. Inset: effective model describing our devices as a gate-tunable QPC shunted by a capacitor.

FREQUENCY-TUNABILITY

We first use a standard two-tone scheme in continuous mode to measure the frequency of the first qubit transition, f_{01}, as a function of the gate voltage. The gate has mainly two effects. First, it changes the Fermi wavelength, thereby opening new conduction channels.

The second effect is a change of the channels' transmission. Experimentally, this is apparent as oscillations in the normal state resistance, R_N, of the junction and is referred to as electronic Fabry-Pérot interferences [20]. This effect is found in high quality devices hosting ballistic carrier transport.

The $f_{01}\,(V_\mathrm{g})$ data for devices Q_1 and Q_2 are shown in Figs. 3(a,b), respectively. When V_g hits the crossover between the hole- and electron-conduction regimes in graphene, i.e. at the charge neutrality point (CNP), the critical current reaches a minimal value, resulting in maximal Josephson inductance L_J and minimal f_{01}. Moving away from the CNP, f_{01} increases in both devices. In device Q_1, a strong asymmetry in with respect to V_CNP is observed. For $V_\mathrm{g} > V_\mathrm{CNP}$ (n-doped graphene), f_{01} increases quickly with charge carrier density, from ~ 3 to ~ 9 GHz within < 1 V only. Such sensitive tunability is appealing for applications that require fast frequency tuning of the transition, such as tunable coupling [31] or Z-gate [32]. For $V_\mathrm{g} < V_\mathrm{CNP}$ (p-doped graphene), f_{01} increases more progressively while oscillating. Similar behaviour was reported in Ref. [16] and is reminiscent of what is observed when measuring the critical current of such graphene Josephson junctions [33] (see also Supplemental Material [28]). The asymmetry is attributed to the electron doping induced by the Ti/Al contacts, which decreases the transmission at the interfaces in the p-doped regime of graphene because of the presence of a pn junction [20, 34].

In device Q_2, we also observe a large f_{01} tunability (several GHz) and oscillations but no clear asymmetry between the p-doped and n-doped regimes. We attribute this to the different gate geometry. As illustrated in Fig. 1(d), in device Q_2 the narrow gate only partly covers the junction, presumably resulting in a more complex electrostatic landscape, and charge density profile, than in Q_1.

TUNABLE CHARGE DISPERSION AND ANHARMONICITY

While the charge dispersion, i.e. $\delta f_{01} = f_{01}\,(n_\mathrm{g} = 0) - f_{01}\,(n_\mathrm{g} = 0.5)$, is too small to be measured in device Q_1, owing to the large $E_\mathrm{J}/E_\mathrm{C}$ in this device (> 15), it is appreciable in device Q_2, whose $E_\mathrm{J}/E_\mathrm{C}$ ratio falls in a lower range (2 to 4) due to the larger designed E_C. Although this is certainly antinomic with a long-lasting coherence (hence, not a desirable property for a qubit), with this device we are able to show that δf_{01} can be reduced, not only by circuit geometry (i.e. by setting an $E_\mathrm{J}/E_\mathrm{C}$ ratio by design), but via the action of

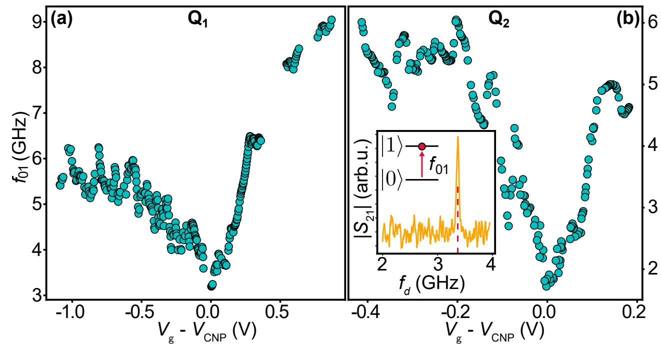

FIG. 3. Gate-tunability of the qubit frequency. (a) Qubit frequency, f_{01}, as a function of the gate voltage, V_{g} for device Q_1. The charge neutrality point (CNP) is found at $V_{\mathrm{CNP}} \simeq$-1.81 eV. (b) Same kind of data for device Q_2. The inset shows a typical two-tone measurement of the qubit dispersively coupled to a readout resonator. When the drive tone frequency, f_{d}, matches the qubit frequency, the qubit is excited from state $|0\rangle$ to state $|1\rangle$. The resonant frequency of the resonator is shifted accordingly and probed by a change in the amplitude, $|S_{21}|$, of the readout tone.

the topgate on graphene, which modifies E_{J}.

Figure 4(a) presents the result of the two-tone measurement, as a function of n_{g}, for $V_{\mathrm{g}} = 0.41$ V, from which we deduce a $\delta f_{01} = 614 \pm 4$ MHz. The energy levels appear in the form of two branches, each corresponding to a different parity of the charge states. This is due to quasiparticle poisonning, occuring at much faster time-scale than the few-seconds duration of a full sweep of f_{d} (specific designs, beyond the scope of the present work, exist to reduce poisonning [35]).

To study the effect of the gate voltage, we select a low $E_{\mathrm{J}}/E_{\mathrm{C}}$ near the CNP of device Q_2. Varying V_{g} within a 100 mV range, we find that δf_{01} values span between ~ 800 and ~ 350 MHz. This is represented in Fig. 4(c) (cyan data points) as a function of $E_{\mathrm{J}}/E_{\mathrm{C}}$, which increases by a factor two with V_{g}, while the transmission stays in the range 0.6 to 0.8. This is consistent with what has been derived from measurements of the current-phase relation (CPR) of graphene Josephson junctions [36–38] and tunnel spectroscopy of the Andreev levels dispersion [39]. Importantly, our model indicates that the large transmission values, compared to a tunnel junction, translate into a substantial reduction of the charge dispersion, as illustrated in Fig. 4(c) (and further discussed in Supplemental Material [28]). This trend is not restricted to graphene, and also applies in gatemon qubits based on InAs nanowires weak links [30, 40]. In a charge qubit with a relatively small $E_{\mathrm{J}}/E_{\mathrm{C}}$ ratio (i.e.

away from the transmon regime), as is the case of our Q_2 device, this could be used to mitigate the sensitivity to charge noise while preserving a large anharmonicity, the latter being required for fast control of the qubit [41]. In our top-gated graphene-based qubit, the channels' transmission can further be increased with V_g, and the δf_{01} reduced accordingly, as also shown in Fig. 4(c).

In Figure 4(c), the E_J extracted from our effective model varies from about 1 to 2 GHz. These are smaller than that the 10 GHz value expected for a single, full-transmission channel between two Al electrodes (200 μeV superconducting gap), suggesting $N_C < 1$ in the V_g range of Fig. 4(c). The sub-unit values suggest that other models might be more relevant in this low-doping region (close to CNP), e.g. a resonant-level picture taking into account an energy-dependent transmission [42].

From Figure 4(c) [i.e. from the experimental qubit first transition frequency f_{01} and charge dispersion δf_{01} of Fig. 4(a)], our model predicts an effective transmission $\tau = 0.73$ and $E_J/E_C = 2.79$. Feeding these numbers into Hamiltonian 1, we derive $f_{02}(n_g)$. The values reproduce remarkably well the evolution of the transition to the second excited state [Fig. 4(b)], further confirming that our short-junction-limit model provides a relevant description of our system.

We finally turn to the qubit's anharmonicity α in device Q_1, which we experimentally determine as a function of V_g by comparing f_{01} and f_{02} (here obtained by a two-photon process at large power [43]), i.e. $\alpha = 2\left(\frac{f_{02}}{2} - f_{01}\right)$. The corresponding data are shown in Supplemental Material [28], and are represented as a function of the inferred $E_J\left(V_g\right)/E_C$ ratio using our model in Fig. 5(a,b) in the n-doped and p-doped regimes of graphene, respectively. We first note that $-\alpha$ remains small, never exceeding 350 MHz, which is close to the charging energy of the device ($E_C/h = 343$ MHz). Values lower than E_C are not unusual with gatemon qubits, generally operated in the transmon regime, and signal a close-to-harmonic Josephson potential tied to a high channel transmission [43–48]. Away from the low-transmission limit, the nonzero-length (L) weak link should additionally further reduce α [49]. The (small) $-\alpha$ presents strong relative variations, reaching values below 100 MHz. For $V_g < V_{CNP}$, i.e. in the p-doped conduction regime, Fig. 5(a) reveals large reproducible anharmonicity fluctuations, which seem to be correlated to those in f_{01} [Fig. 3(a)]. These aperiodic oscillations are linked to Fabry-Pérot-like interferences of ballistic electronic states, typically observed in the normal state resistance of such mesoscopic device. According to

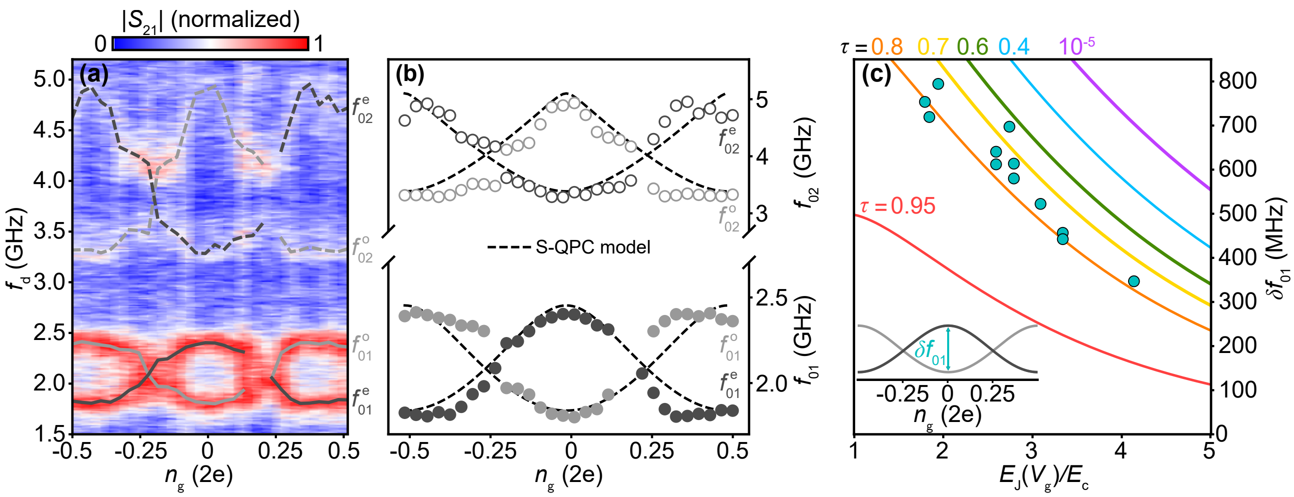

FIG. 4. Qubit spectrum and charge dispersion in device Q_2. (a) Two-tone measurement of the first two qubit transitions as a function of the charge offset, n_g, at $V_g = 0.41$ V. Solid and dashed lines represent the fitted frequency of the two charge parities (odd and even, labeled 'o' and 'e') of the $|0\rangle$-$|1\rangle$ and $|0\rangle$-$|2\rangle$ transitions. (b) Reconstruction of the qubit spectrum at $V_g = 0.41$ V using only the set of $(\delta f_{01}, f_{01})$ values derived from the experimental data. (c) Charge dispersion, δf_{01}, as a function of $E_J(V_g)/E_C$, extracted from data such as in (a) (as shown in the inset), varying V_g from 400 mV to 486 mV. The coloured solid lines represent the charge dispersion predicted by Hamiltonian 1 for different values of transmission.

our model, these fluctuations trace back to large variations of the effective transmission of the junction with V_g, from 0.2 to 1. In contrast, in the n-doped conduction regime in graphene [Fig. 5(b)], α exhibits less fluctuations, with a global tendency to decrease with $E_J(V_g)$ towards a small fraction of the charging energy. At this limit, our model predicts a transmission close to unity. Overall, covering a broad range of E_J/E_C values (15 to 90) through a V_g excursion of less than 1 V, we demonstrate a tuning of the qubit's anharmonicity from $-E_C/h$ to $-E_C/4h$. To retain a large enough anharmonicity while conserving gate-tunability, it has been shown that other designs, such as the flux-tunable transmon [7], or the fluxonium [50], could favorably integrate gate-tunable weak links.

CONCLUSION

We have used Josephson junctions with a top-gated graphene weak link to build charge qubits operating in a broad range of E_J/E_C ratios and having highly gate-tunable energy

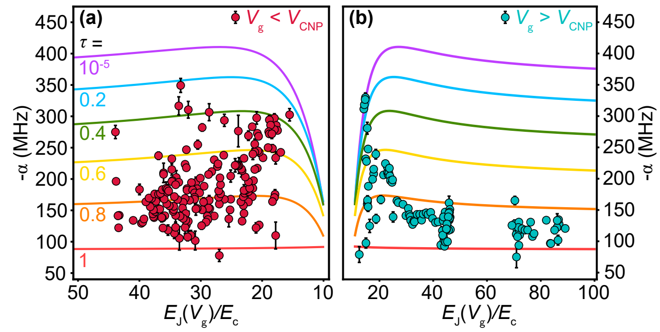

FIG. 5. Gate-dependent anharmonicity α in device Q_1 as a function of $E_J(V_g)/E_C$, in the p- (a) and n-doped (b) conduction regime of graphene. The solid lines are the model predictions for a set of transmissions.

spectrum. The fundamental qubit transition is sensitively tuned, by several GHz, via the topgate voltage. Designing a device with small E_J/E_C, which is intrinsically prone to significant charge dispersion, we show that a high effective transmission of the Josephson junction mitigates this charge dispersion, which can be further reduced by in-situ increasing E_J, again via V_g. The anharmonicity of our graphene-based qubits at large E_J/E_C is relatively small, partly due to the high transmission of the junctions, but can be increased using a more complex design in the future [7, 50]. To rationalize our results and model a graphene superconducting qubit, we have used and discussed a model initially introduced to describe superconducting quantum point contacts, which takes into account the ground and excited states of the Andreev bound states in the weak link. The model has two key parameters: the Josephson energy and effective transmission of the conduction channels in the weak link. It quantitatively account for our results, except close to the charge neutrality point where the assumption of an energy-independent transmission seems not to hold. A resonant-level model might be more appropriate to describe this specific regime of only a few conducting channels [42]. Our work highlights graphene-based hybrid junctions as promising candidates for qubits with low noise susceptibility, which, together with the efficient gate-tunability, holds promises for advanced functionnalities in superconducting quantum circuits. A more robust control of the channels' transmission using local gates near the superconducting electrodes [51–55] towards a complete suppression of charge dispersion might further improve the quantum coherence of such circuits.

ACKNOWLEDGMENTS

We acknowledge the staff of the Nanofab cleanroom of Institut Néel for help with device fabrication. We thank Richard Haettel for assistance in device annealing, Simon Le Denmat for atomic force microscopy and Aloïs Arrighi for sharing the PDMS transfer technique. We acknowledge the work of Julien Jarreau, Laurent Del-Rey and Didier Dufeu for the design and fabrication of the sample holders and other mechanical pieces used in the cryogenic system. We thank Denis M. Basko for fruitful discussions and help with numerical implementations of the models. We also thank Landry Bretheau, Sergey Frolov, Tereza Vakhtel for discussions. This work was supported by the French National Research Agency (ANR) in the framework of the Graphmon project (ANR-19-CE47-0007). This work benefited from a French government grant managed by the ANR agency under the 'France 2030 plan', with reference ANR-22-PETQ-0003. K.W. and T.T. acknowledge support from the JSPS KAKENHI (Grant Numbers 21H05233 and 23H02052) and World Premier International Research Center Initiative (WPI), MEXT, Japan.

DATA AVAILABILITY STATEMENT

The supporting data for this article are openly available from the Zenodo repository with the identifier https://doi.org/10.5281/zenodo.15511640[56].

[1] C. Macklin, K. O'Brien, D. Hover, M. E. Schwartz, V. Bolkhovsky, X. Zhang, W. D. Oliver, and I. Siddiqi, A near–quantum-limited josephson traveling-wave parametric amplifier, Science **350**, 307 (2015).

[2] A. Somoroff, Q. Ficheux, R. A. Mencia, H. Xiong, R. Kuzmin, and V. E. Manucharyan, Millisecond coherence in a superconducting qubit, Phys. Rev. Lett. **130**, 267001 (2023).

[3] B. Ho Eom, P. K. Day, H. G. LeDuc, and J. Zmuidzinas, A wideband, low-noise superconducting amplifier with high dynamic range, Nat. Phys. **8**, 623 (2012).

[4] P. Winkel, K. Borisov, L. Grünhaupt, D. Rieger, M. Spiecker, F. Valenti, A. V. Ustinov, W. Wernsdorfer, and I. M. Pop, Implementation of a transmon qubit using superconducting granular aluminum, Phys. Rev. X **10**, 031032 (2020).

[5] L. Grünhaupt, M. Spiecker, D. Gusenkova, N. Maleeva, S. T. Skacel, I. Takmakov, F. Valenti, P. Winkel, H. Rotzinger, W. Wernsdorfer, A. V. Ustinov, and I. M. Pop, Granular aluminium as a superconducting material for high-impedance quantum circuits, Nat. Mater. **18**, 816 (2019).

[6] T. W. Larsen, K. D. Petersson, F. Kuemmeth, T. S. Jespersen, P. Krogstrup, J. Nygård, and C. M. Marcus, Semiconductor-Nanowire-Based Superconducting Qubit, Phys. Rev. Lett. **115**, 127001 (2015).

[7] G. de Lange, B. van Heck, A. Bruno, D. J. van Woerkom, A. Geresdi, S. R. Plissard, E. P. A. M. Bakkers, A. R. Akhmerov, and L. DiCarlo, Realization of Microwave Quantum Circuits Using Hybrid Superconducting-Semiconducting Nanowire Josephson Elements, Phys. Rev. Lett. **115**, 127002 (2015).

[8] L. Casparis, M. R. Connolly, M. Kjaergaard, N. J. Pearson, A. Kringhøj, T. W. Larsen, F. Kuemmeth, T. Wang, C. Thomas, S. Gronin, G. C. Gardner, M. J. Manfra, C. M. Marcus, and K. D. Petersson, Superconducting gatemon qubit based on a proximitized two-dimensional electron gas, Nat. Nanotechnol. **13**, 915 (2018).

[9] D. Feldstein-Bofill, Z. Sun, C. Wied, S. Singh, B. D. Isakov, S. Krøjer, J. Hastrup, A. Gyenis, and M. Kjaergaard, Gatemon qubit revisited for improved reliability and stability (2024), arXiv:2412.11611.

[10] G. Butseraen, A. Ranadive, N. Aparicio, K. Rafsanjani Amin, A. Juyal, M. Esposito, K. Watanabe, T. Taniguchi, N. Roch, F. Lefloch, and J. Renard, A gate-tunable graphene Josephson parametric amplifier, Nat. Nanotechnol. **17**, 1153–1158 (2022).

[11] J. Sarkar, K. V. Salunkhe, S. Mandal, S. Ghatak, A. H. Marchawala, I. Das, K. Watanabe, T. Taniguchi, R. Vijay, and M. M. Deshmukh, Quantum noise limited microwave amplification using a graphene Josephson junction, Nat. Nanotechnol. **17**, 1147–1152 (2022).

[12] D. Phan, P. Falthansl-Scheinecker, U. Mishra, W. Strickland, D. Langone, J. Shabani, and A. Higginbotham, Gate-tunable superconductor-semiconductor parametric amplifier, Phys. Rev. Appl. **19**, 064032 (2023).

[13] Z. Hao, T. Shaw, M. Hatefipour, W. M. Strickland, B. H. Elfeky, D. Langone, J. Shabani, and S. Shankar, Kerr nonlinearity and parametric amplification with an Al-InAs superconductor–semiconductor Josephson junction, Appl. Phys. Lett. **124**, 254003 (2024).

[14] W. M. Strickland, L. J. Baker, J. Lee, K. Dindial, B. H. Elfeky, P. J. Strohbeen, M. Hatefipour, P. Yu, I. Levy, J. Issokson, V. E. Manucharyan, and J. Shabani, Characterizing losses in inas two-dimensional electron gas-based gatemon qubits, Phys. Rev. Res. **6**, 023094 (2024).

[15] E. Kiyooka, C. Tangchingchai, L. Noirot, A. Leblanc, B. Brun, S. Zihlmann, R. Maurand, V. Schmitt, É. Dumur, J.-M. Hartmann, F. Lefloch, and S. De Franceschi, Gatemon qubit on a germanium Quantum-Well heterostructure, Nano Lett. **25**, 562 (2025).

[16] J. I.-J. Wang, D. Rodan-Legrain, L. Bretheau, D. L. Campbell, B. Kannan, D. Kim, M. Kjaergaard, P. Krantz, G. O. Samach, F. Yan, J. L. Yoder, K. Watanabe, T. Taniguchi, T. P. Orlando, S. Gustavsson, P. Jarillo-Herrero, and W. D. Oliver, Coherent control of a hybrid superconducting circuit made with graphene-based van der Waals heterostructures, Nat. Nanotechnol. **14**, 120–125 (2019).

[17] J. G. Kroll, W. Uilhoorn, K. L. van der Enden, D. de Jong, K. Watanabe, T. Taniguchi, S. Goswami, M. C. Cassidy, and L. P. Kouwenhoven, Magnetic field compatible circuit quantum electrodynamics with graphene josephson junctions, Nature Communications **9**, 4615 (2018).

[18] L. Casparis, T. W. Larsen, M. S. Olsen, F. Kuemmeth, P. Krogstrup, J. Nygård, K. D. Petersson, and C. M. Marcus, Gatemon benchmarking and two-qubit operations, Phys. Rev. Lett. **116**, 150505 (2016).

[19] H. B. Heersche, P. Jarillo-Herrero, J. B. Oostinga, L. M. K. Vandersypen, and A. F. Morpurgo, Bipolar supercurrent in graphene, Nature **446**, 56 (2007).

[20] V. E. Calado, S. Goswami, G. Nanda, M. Diez, A. R. Akhmerov, K. Watanabe, T. Taniguchi, T. M. Klapwijk, and L. M. K. Vandersypen, Ballistic Josephson junctions in edge-contacted graphene, Nat. Nanotechnol. **10**, 761 (2015).

[21] F. Nichele, E. Portolés, A. Fornieri, A. M. Whiticar, A. C. C. Drachmann, S. Gronin, T. Wang, G. C. Gardner, C. Thomas, A. T. Hatke, M. J. Manfra, and C. M. Marcus, Relating andreev bound states and supercurrents in hybrid josephson junctions, Phys. Rev. Lett. **124**, 226801 (2020).

[22] M. Hinderling, S. C. ten Kate, M. Coraiola, D. Haxell, M. Stiefel, M. Mergenthaler, S. Paredes, S. Bedell, D. Sabonis, and F. Nichele, Direct microwave spectroscopy of andreev bound states in planar Ge josephson junctions, PRX Quantum **5**, 030357 (2024).

[23] G.-H. Park, W. Lee, S. Park, K. Watanabe, T. Taniguchi, G. Y. Cho, and G.-H. Lee, Controllable andreev bound states in bilayer graphene josephson junctions from short to long junction limits, Phys. Rev. Lett. **132**, 226301 (2024).

[24] B. H. Elfeky, K. Dindial, D. S. Brandão, B. m. c. Pekerten, J. Lee, W. M. Strickland, P. J. Strohbeen, A. Danilenko, L. Baker, M. Mikalsen, W. Schiela, Z. Liang, J. Issokson, I. Levy, I. Žutić, and J. Shabani, Microwave andreev bound state spectroscopy in a semiconductor-based planar josephson junction, Phys. Rev. Res. **7**, 013248 (2025).

[25] F. Zhang, A. S. Rashid, M. T. Ahari, W. Zhang, K. M. Ananthanarayanan, R. Xiao, G. J. de Coster, M. J. Gilbert, N. Samarth, and M. Kayyalha, Andreev processes in mesoscopic multiterminal graphene josephson junctions, Phys. Rev. B **107**, L140503 (2023).

[26] C. Ciaccia, R. Haller, A. C. C. Drachmann, T. Lindemann, M. J. Manfra, C. Schrade, and C. Schönenberger, Charge-4e supercurrent in a two-dimensional InAs-Al superconductor-semiconductor heterostructure, Commun. Phys. **7**, 41 (2024).

[27] R. Haller, M. Osterwalder, G. Fülöp, J. Ridderbos, M. Jung, and C. Schönenberger, ac josephson effect in a gate-tunable cd_3as_2 nanowire superconducting weak link, Phys. Rev. B **108**, 094514 (2023).

[28] See Supplemental Material at [url] for details about device fabrication, discussions about the number of conduction channels, the derivation of the model as well as additional measurements, which includes Refs. [16, 20, 29, 39, 44, 57–65].

[29] D. A. Ivanov and M. V. Feigel'man, Two-level hamiltonian of a superconducting quantum point contact, Phys. Rev. B **59**, 8444 (1999).

[30] A. Kringhøj, B. van Heck, T. W. Larsen, O. Erlandsson, D. Sabonis, P. Krogstrup, L. Casparis, K. D. Petersson, and C. M. Marcus, Suppressed charge dispersion via resonant tunneling in a single-channel transmon, Phys. Rev. Lett. **124**, 246803 (2020).

[31] R. McDermott, R. W. Simmonds, M. Steffen, K. B. Cooper, K. Cicak, K. D. Osborn, S. Oh, D. P. Pappas, and J. M. Martinis, Simultaneous state measurement of coupled josephson phase qubits, Science **307**, 1299 (2005).

[32] M. Steffen, M. Ansmann, R. McDermott, N. Katz, R. C. Bialczak, E. Lucero, M. Neeley, E. M. Weig, A. N. Cleland, and J. M. Martinis, State tomography of capacitively shunted phase qubits with high fidelity, Phys. Rev. Lett. **97**, 050502 (2006).

[33] J. Park, J. H. Lee, G.-H. Lee, Y. Takane, K.-I. Imura, T. Taniguchi, K. Watanabe, and H.-J. Lee, Short ballistic josephson coupling in planar graphene junctions with inhomogeneous carrier doping, Phys. Rev. Lett. **120**, 077701 (2018).

[34] G. Giovannetti, P. A. Khomyakov, G. Brocks, V. M. Karpan, J. van den Brink, and P. J. Kelly, Doping graphene with metal contacts, Phys. Rev. Lett. **101**, 026803 (2008).

[35] X. Pan, Y. Zhou, H. Yuan, L. Nie, W. Wei, L. Zhang, J. Li, S. Liu, Z. H. Jiang, G. Catelani, L. Hu, F. Yan, and D. Yu, Engineering superconducting qubits to reduce quasiparticles and charge noise, Nat. Commun. **13**, 7196 (2022).

[36] G.-H. Lee, S. Kim, S.-H. Jhi, and H.-J. Lee, Ultimately short ballistic vertical graphene josephson junctions, Nat. Commun. **6**, 6181 (2015).

[37] R. Jha, M. Endres, K. Watanabe, T. Taniguchi, M. Banerjee, C. Schönenberger, and P. Karnatak, Large tunable kinetic inductance in a twisted graphene superconductor, arXiv preprint arXiv:2403.02320 (2024).

[38] S. Messelot, N. Aparicio, E. de Seze, E. Eyraud, J. Coraux, K. Watanabe, T. Taniguchi, and J. Renard, Direct measurement of a $\sin(2\varphi)$ current phase relation in a graphene superconducting quantum interference device, Phys. Rev. Lett. **133**, 106001 (2024).

[39] L. Bretheau, J. I.-J. Wang, R. Pisoni, K. Watanabe, T. Taniguchi, and P. Jarillo-Herrero, Tunnelling spectroscopy of Andreev states in graphene, Nat. Phys. **13**, 756 (2017).

[40] A. Bargerbos, W. Uilhoorn, C.-K. Yang, P. Krogstrup, L. P. Kouwenhoven, G. de Lange, B. van Heck, and A. Kou, Observation of vanishing charge dispersion of a nearly open superconducting island, Phys. Rev. Lett. **124**, 246802 (2020).

[41] P. Krantz, M. Kjaergaard, F. Yan, T. P. Orlando, S. Gustavsson, and W. D. Oliver, A quantum engineer's guide to superconducting qubits, Appl. Phys. Rev. **6**, 021318 (2019).

[42] P. D. Kurilovich, V. D. Kurilovich, V. Fatemi, M. H. Devoret, and L. I. Glazman, Microwave response of an andreev bound state, Phys. Rev. B **104**, 174517 (2021).

[43] A. Kringhøj, L. Casparis, M. Hell, T. W. Larsen, F. Kuemmeth, M. Leijnse, K. Flensberg, P. Krogstrup, J. Nygård, K. D. Petersson, and C. M. Marcus, Anharmonicity of a superconducting qubit with a few-mode josephson junction, Phys. Rev. B **97**, 060508 (2018).

[44] A. Hertel, M. Eichinger, L. O. Andersen, D. M. van Zanten, S. Kallatt, P. Scarlino, A. Kringhøj, J. M. Chavez-Garcia, G. C. Gardner, S. Gronin, M. J. Manfra, A. Gyenis, M. Kjaergaard, C. M. Marcus, and K. D. Petersson, Gate-tunable transmon using selective-

area-grown superconductor-semiconductor hybrid structures on silicon, Phys. Rev. Appl. **18**, 034042 (2022).

[45] H. Zheng, L. Y. Cheung, N. Sangwan, A. Kononov, R. Haller, J. Ridderbos, C. Ciaccia, J. H. Ungerer, A. Li, E. P. A. M. Bakkers, A. Baumgartner, and C. Schönenberger, Coherent control of a few-channel hole type gatemon qubit, Nano Lett. **24**, 7173 (2023).

[46] E. Zhuo, Z. Lyu, X. Sun, A. Li, B. Li, Z. Ji, J. Fan, E. P. A. M. Bakkers, X. Han, X. Song, F. Qu, G. Liu, J. Shen, and L. Lu, Hole-type superconducting gatemon qubit based on Ge/Si core/shell nanowires, npj Quantum Inf. **9**, 51 (2023).

[47] O. Sagi, A. Crippa, M. Valentini, M. Janik, L. Baghumyan, G. Fabris, L. Kapoor, F. Hassani, J. Fink, S. Calcaterra, D. Chrastina, G. Isella, and G. Katsaros, A gate tunable transmon qubit in planar Ge, Nat. Commun. **15**, 6400 (2024).

[48] E. Kiyooka, C. Tangchingchai, L. Noirot, A. Leblanc, B. Brun, S. Zihlmann, R. Maurand, V. Schmitt, É. Dumur, J.-M. Hartmann, F. Lefloch, and S. De Franceschi, Gatemon qubit on a germanium Quantum-Well heterostructure, Nano Lett. **25**, 562 (2025).

[49] V. Fatemi, P. D. Kurilovich, A. R. Akhmerov, and B. van Heck, Nonlinearity of transparent sns weak links decreases sharply with length, arXiv preprint arXiv:2410.01913 (2024).

[50] W. M. Strickland, B. H. Elfeky, L. Baker, A. Maiani, J. Lee, I. Levy, J. Issokson, A. Vrajitoarea, and J. Shabani, Gatemonium: A voltage-tunable fluxonium, PRX Quantum **6**, 010326 (2025).

[51] M. Eich, F. c. v. Herman, R. Pisoni, H. Overweg, A. Kurzmann, Y. Lee, P. Rickhaus, K. Watanabe, T. Taniguchi, M. Sigrist, T. Ihn, and K. Ensslin, Spin and valley states in gate-defined bilayer graphene quantum dots, Phys. Rev. X **8**, 031023 (2018).

[52] R. Pisoni, Z. Lei, P. Back, M. Eich, H. Overweg, Y. Lee, K. Watanabe, T. Taniguchi, T. Ihn, and K. Ensslin, Gate-tunable quantum dot in a high quality single layer mos2 van der waals heterostructure, Appl. Phys. Lett. **112**, 123101 (2018).

[53] J. Li, H. Wen, K. Watanabe, T. Taniguchi, and J. Zhu, Gate-controlled transmission of quantum hall edge states in bilayer graphene, Phys. Rev. Lett. **120**, 057701 (2018).

[54] V. Jangir, D. Shah, S. Samanta, S. Rastogi, H. E. Beere, D. A. Ritchie, K. Das Gupta, and S. Mahapatra, Preserving coulomb blockade in transport spectroscopy of quantum dots by dynamical tunnel barrier compensation, Appl. Phys. Lett. **125**, 263503 (2024).

[55] A. Bordin, F. J. Bennebroek Evertsz', G. O. Steffensen, T. Dvir, G. P. Mazur, D. van Driel, N. van Loo, J. C. Wolff, E. P. A. M. Bakkers, A. L. Yeyati, and L. P. Kouwenhoven, Impact of andreev bound states within the leads of a quantum dot josephson junction, Phys. Rev. X **15**, 011046 (2025).

[56] N. Aparicio, S. Messelot, E. Orozco, E. Eyraud, T. Taniguchi, K. Watanabe, J. Coraux, and J. Renard, Data and numerical model implentation for "Gate- tunable spectrum and charge dispersion mitigation in a graphene superconducting qubit", 10.5281/zenodo.15511640 (2025).

[57] P. J. Zomer, M. H. D. Guimarães, J. C. Brant, N. Tombros, and B. J. van Wees, Fast pick up technique for high quality heterostructures of bilayer graphene and hexagonal boron nitride, Appl. Phys. Lett. **105**, 013101 (2014).

[58] K. Kim, M. Yankowitz, B. Fallahazad, S. Kang, H. C. P. Movva, S. Huang, S. Larentis, C. M. Corbet, T. Taniguchi, K. Watanabe, S. K. Banerjee, B. J. LeRoy, and E. Tutuc, Van der waals heterostructures with high accuracy rotational alignment, Nano Lett. **16**, 1989 (2016).

[59] L. Wang, I. Meric, P. Y. Huang, Q. Gao, Y. Gao, H. Tran, T. Taniguchi, K. Watanabe, L. M. Campos, D. A. Muller, J. Guo, P. Kim, J. Hone, K. L. Shepard, and C. R. Dean, One-Dimensional Electrical Contact to a Two-Dimensional Material, Science **342**, 614 (2013).

[60] A. Laturia, M. L. Van de Put, and W. G. Vandenberghe, Dielectric properties of hexagonal boron nitride and transition metal dichalcogenides: from monolayer to bulk, npj 2D Mater. Appl. **2**, 6 (2018).

[61] J. I.-J. Wang, M. A. Yamoah, Q. Li, A. H. Karamlou, T. Dinh, B. Kannan, J. Braumüller, D. Kim, A. J. Melville, S. E. Muschinske, B. M. Niedzielski, K. Serniak, Y. Sung, R. Winik, J. L. Yoder, M. E. Schwartz, K. Watanabe, T. Taniguchi, T. P. Orlando, S. Gustavsson, P. Jarillo-Herrero, and W. D. Oliver, Hexagonal boron nitride as a low-loss dielectric for superconducting quantum circuits and qubits, Nat. Mater. **21**, 398 (2022).

[62] J. Koch, T. M. Yu, J. Gambetta, A. A. Houck, D. I. Schuster, J. Majer, A. Blais, M. H. Devoret, S. M. Girvin, and R. J. Schoelkopf, Charge-insensitive qubit design derived from the Cooper pair box, Phys. Rev. A **76**, 042319 (2007).

[63] T. Vakhtel and B. van Heck, Quantum phase slips in a resonant josephson junction, Phys. Rev. B **107**, 195405 (2023).

[64] A. Zazunov, V. S. Shumeiko, E. N. Bratus', J. Lantz, and G. Wendin, Andreev level qubit, Phys. Rev. Lett. **90**, 087003 (2003).

[65] D. I. Schuster, A. Wallraff, A. Blais, L. Frunzio, R.-S. Huang, J. Majer, S. M. Girvin, and R. J. Schoelkopf, ac stark shift and dephasing of a superconducting qubit strongly coupled to a cavity field, Phys. Rev. Lett. **94**, 123602 (2005).

[66] F. Pizzocchero, L. Gammelgaard, B. S. Jessen, J. M. Caridad, L. Wang, J. Hone, P. Bøggild, and T. J. Booth, The hot pick-up technique for batch assembly of van der waals heterostructures, Nat. Commun. **7**, 11894 (2016).

[67] I. O. Kulik, Macroscopic quantization and the proximity effect in s-n-s junctions, Sov. Phys. JETP **30**, 944 (1970).

[68] C. W. J. Beenakker and H. van Houten, Josephson current through a superconducting quantum point contact shorter than the coherence length, Phys. Rev. Lett. **66**, 3056 (1991).

[69] M. Titov and C. W. J. Beenakker, Josephson effect in ballistic graphene, Phys. Rev. B **74**, 041401 (2006).

END MATTER

Appendix A: Device fabrication

Device fabrication comprises four main steps (eight individual steps in total, see Supplemental Material [28]). First, we define the aluminum superconducting circuit (transmission line, resonator, qubit, drive line, and gate) via e-beam lithography of a thin metal film (80 nm) deposited onto a high-resistivity silicon substrate. Second, we assemble the graphene weak link. To do so, we encapsulate graphene between two hexagonal boron nitride (h-BN) layers ($\sim$ 30 nm-thick each) using a dry transfer technique [66], to minimize the amount of airborne species in contact with graphene, which otherwise would harm the devices' performance. Third, graphene is side-contacted to Al electrodes (80 nm), after a buffer Ti layer (5 nm) has been deposited to improve the transmission of the metal/graphene contacts [59]. To ensure a good electrical connection between the Al made in different steps, we use in-situ Ar milling. The (graphene) weak link is 350 nm-wide and 350 nm-long. The fourth step is the fabrication of the topgate. For Q_1, we use an extra layer of h-BN to prevent any contact with the side electrodes, above which a 1 μm-wide Al electrode is defined by e-beam lithography followed by e-beam evaporation (80 nm). The topgate here spans the whole Josephson junction [Fig. 1(b,c)]. On the contrary, for Q_2, we used no extra h-BN layer but a narrow, 100 nm-wide finger gate directly deposited on top of the h-BN/graphene/h-BN heterostructure [Fig. 1(d)]. This requires an accurate alignment in e-beam lithography but potentially improves device cleanliness as no extra h-BN deposition is needed.

TABLE I. Capacitances, coupling quality factor, and charging energy calculated for the two devices Q_1 and Q_2 from electrostatic and electromagnetic simulations (Ansys Maxwell electrostatic and Sonnet electromagnetic simulations).

	C_c (fF)	C_{qr} (fF)	C_S (fF)	C_d (aF)	C_g (fF)	Q_c	E_C/h (MHz)
Q_1	3.80	4.46	50.7	176	1.03	1.30×10^4	343
Q_2	12.7	3.71	32.5	168	1.14	4.09×10^3	516

Appendix B: Josephson junction models

In a semiconductor-superconductor weak link, the charge carrier density is a crucial parameter that will determine the number of channels contributing to the supercurrent, some of which can have high transmission ($\hat{H}_{TJ}$ accounts only for low-probability tunneling processes). Several models have been used to describe highly transmitting junctions with a small number of channels. In the so-called short junction limit of a single ABS per conduction channel (i.e. when the length L is small compared to the superconducting coherence length in the electrodes ξ), the energy of a single ABS is given by [39, 67–69]

$$E_{\pm} = \pm\Delta\sqrt{1 - \tau \sin\left(\frac{\varphi}{2}\right)^2} \tag{B1}$$

where '±' denotes the two branches of the ABS pair, Δ is the gap of the superconducting electrodes, and τ is the channel transmission. Assuming that only the ground energy ABS contributes, leads to the Josephson Hamiltonian $\hat{H}_{ABS^-} = -\Delta\sqrt{1 - \tau \sin\left(\frac{\hat{\varphi}}{2}\right)^2}$, which approximates well to the tunnel Hamiltonian $\hat{H}_{TJ}$ in the limit $\tau \ll 1$, for $E_J = \frac{\Delta\tau}{4}$ [43, 45]. This model, limited to the ABS ground state, has been used to describe gatemon qubits based on III-V nanowires, wherein transmission through resonant levels indeed can lead to high transmission [7, 43]. Here, we propose a model to describe the complete ABS-pair.

The Josephson potential of a quantum point contact at perfect (solid orange line) and intermediate (dashed black line) transmission taking into account the ABSs is represented in Fig. 2(b). The two ABS branches across the superconducting gap are only well-separated for small τ values. In other words, when transmission approaches unity, a proper description of the system must include both branches, as Landau-Zener like transitions between the ground and excited ABSs, are susceptible to occur where the two branches are the closest, i.e. $\varphi = \pi \ [2\pi]$ [63]. Importantly, doing so to model superconducting quantum point contacts (S-QPC) [30, 40] or resonant tunneling [63], one predicts a strong reduction of the charge dispersion, in case of a high transmission, owing to the suppression of 2π-quantum phase slips (2π-QPSs).